

Solution and Crystal Structures of a Sperm Whale Myoglobin Triple Mutant That Mimics the Sulfide-binding Hemoglobin from *Lucina pectinata**

(Received for publication, August 25, 1997, and in revised form, February 6, 1998)

Bao D. Nguyen, Xuefeng Zhao, Krishnamurthi Vyas, and Gerd N. La Mar‡

From the Department of Chemistry, University of California, Davis, California 95616

R. Ashley Lile, Eric Allen Brucker§, George N. Phillips, Jr., and John S. Olson

From the Department of Biochemistry and Cell Biology and the W. M. Keck Center for Computational Biology, Rice University, Houston, Texas 77005-1892

Jonathan B. Wittenberg

From the Department of Physiology and Biophysics, Albert Einstein College of Medicine, Bronx, New York 10461

The bivalve mollusc *Lucina pectinata* harbors sulfide-oxidizing chemoautotrophic bacteria and expresses a monomeric hemoglobin I, HbI, with normal O₂, but extraordinarily high sulfide affinity. The crystal structure of aquomet *Lucina* HbI has revealed an active site with three residues not commonly found in vertebrate globins: Phe(B10), Gln(E7), and Phe(E11) (Rizzi, M., Wittenberg, J. B., Coda, A., Fasano, M., Ascenzi, P., and Bolognesi, M. (1994) *J. Mol. Biol.* 244, 86–89). Engineering these three residues into sperm whale myoglobin results in a triple mutant with ~700-fold higher sulfide affinity than for wild-type. The single crystal x-ray structure of the aquomet derivative of the myoglobin triple mutant and the solution ¹H NMR active site structures of the cyanomet derivatives of both the myoglobin mutant and *Lucina* HbI have been determined to examine further the structural origin of their unusually high sulfide affinities. The major differences in the distal pocket is that in the aquomet form the carbonyl of Gln⁶⁴(E7) serves as a H-bond acceptor, whereas in the cyanomet form the amido group acts as H-bond donor to the bound ligand. Phe⁶⁸(E11) is rotated ~90° about χ_2 and located ~1–2 Å closer to the iron atom in the myoglobin triple mutant relative to its conformation in *Lucina* HbI. The change in orientation potentially eliminates the stabilizing interaction with sulfide and, together with the decrease in size of the distal pocket, accounts for the 7-fold lower sulfide affinity of the myoglobin mutant compared with that of *Lucina* HbI.

Despite substantial amino acid sequence variability, the reversible binding of molecular oxygen in myoglobin (Mb)¹ and

hemoglobin (Hb) is achieved by a surprisingly invariant protein folding topology: a heme group imbedded within 7–8 packed α -helices (1, 2). Examination of the more than 300 known sequences of vertebrate Hbs and Mbs and the >130 nonvertebrate globin-like sequences demonstrates that only two residues appear to be conserved, the proximal His at helical position F-8 and the Phe parallel to the heme surface at an interhelical loop, position CD1 (1, 3). The residue considered to be pivotal in the stabilization of the bound O₂ is the one whose side chain can provide a neutral donor for a hydrogen bond with the ligand, such as His or Gln at the distal position E-7. Among vertebrate Mbs and Hbs, His predominates, with Gln occurring only in elephant Mb (4), shark Mb (5), hagfish Hb (6), and the α chain of opossum Hb (7). Although His is also found in the majority of nonvertebrate Hbs and Mbs, Gln is not uncommon and, in addition, other residues may occupy the E-7 position, e.g. Val in *Aplysia* (8) and several other mollusc Mbs (9), Tyr in the Mb from *Paramphistomon epicalitum* (10, 11), and Leu in the monomeric components of *Glycera* Hb (12). Although capable of O₂ binding, a number of the variant globins exhibit some anomalous functional properties. Parallel functional and structural studies on genetically engineered mutants of mammalian Mb have shown that changes in only a very limited number of residues in the distal pocket often transfers the essence of the unusual behavior of the natural genetic variant to the appropriate reference protein mutant (13–17).

Cytoplasmic Hbs occur in many symbiotic associations between bacteria and invertebrates or plants and may have a physiological role in the symbiosis (18–20). The bivalve mollusc *Lucina pectinata*, found in sulfide-rich coastal sediments, harbors sulfide-oxidizing chemoautotrophic bacteria (21, 22). Its abundant cytoplasmic hemoglobins consist of three single-chain components, each having a moderately high affinity for oxygen ($P_{50} = 0.1$ – 0.2 torr), which is achieved, however, by a very different balance of combination and dissociation rates. Reactions of the monomeric HbI with oxygen are rapid, whereas those of HbII and HbIII are extraordinarily slow (23).

bin; MCOSY, magnitude COSY; metMbCN, cyanomet myoglobin; NMR, nuclear magnetic resonance; NOE, nuclear Overhauser effect; NOESY, two-dimensional nuclear Overhauser spectroscopy; ppm, parts per million; TOCSY, two-dimensional total correlation spectroscopy; V68F-Mb, Val⁶⁸(E10)→Phe-Mb; L29F/H64Q/V68F-Mb, Leu²⁹(B10)→Phe, His⁶⁴(E7)→Gln, Val⁶⁸(E11)→Phe-Mb; HbI, monomeric hemoglobin component I; metHbCN, cyanomet-hemoglobin I.

* This work was supported by United States National Institutes of Health Grants HL16087 (to G. N. L.), GM35649 and HL47020 (to J. S. O.), AR40252 (to G. N. P.), and Postdoctoral Fellowship AR08355 (to E. A. B.), the States of Texas Advanced Technology Program Grant 003604-025 (to G. N. P. and J. S. O.), Robert A. Welch Foundation Grants C-612 (to J. S. O.) and C-1142 (to G. N. P.), and the W. M. Keck Center for Computational Biology. The costs of publication of this article were defrayed in part by the payment of page charges. This article must therefore be hereby marked "advertisement" in accordance with 18 U.S.C. Section 1734 solely to indicate this fact.

‡ To whom correspondence should be addressed.

§ Current address: Somatogen, Inc., Boulder, CO 80301.

¹ The abbreviations used are: Mb, myoglobin; Hb, hemoglobin; DSS, 2,2-dimethyl-2-silapentane-5-sulfonate; MbCO, carbonmonoxymyoglo-

Recent crystal structures of *Lucina* aquometHbI and the sulfide bound form (24, 25) have revealed a distal Gln⁶⁴(E7) and Phe²⁹(B10), neither of which is rare among invertebrate Mbs, Hbs. However, the E-11 position is uniquely occupied by Phe rather than the aliphatic amino acids Val, Ile, or Leu. To examine the structural origin of strong sulfide binding in *Lucina* HbI, we have systematically replaced His⁶⁴(E7), Leu²⁹(B10), and Val⁶⁴(E11) with Gln, Phe, and Phe, respectively, in sperm whale myoglobin and then determined the structures of the resulting multiple mutants by NMR and x-ray crystallography. This approach is similar to that used to study the unusual functional properties of *Aplysia* Mb, *Ascaris* Hb, and elephant Mb, and provides comparison between the native protein and the synthetic mimic in two ligation/spin states and between protein structures in crystal and solution (13–17, 26, 27). The NMR studies were pursued to define more carefully the positions of the labile protons of Gln⁶⁴(E7) and their role as hydrogen bond donors to the bound ligand. Both the paramagnetic relaxation and induced dipolar shifts in metMbCN and metHbICN can be used to model the position of distal residues (14–17, 26, 29, 30). The combined NMR and crystallographic results reveal systematic differences between the orientation of Gln⁶⁴(E7) in the aquomet and cyanomet complexes of *Lucina* HbI and L29F/H64Q/V68F-Mb, which demonstrate that Gln⁶⁴(E7) may serve as either a H-bond acceptor or donor to bound ligands and that a difference in the orientation of the Phe⁶⁸(E11) ring may account for the difference in sulfide affinity between *Lucina* HbI and the sperm whale triple mutant Mb mimic.

EXPERIMENTAL PROCEDURES

Protein Preparation—The pUC19 plasmid containing V68F sperm whale myoglobin was made by Egeberg *et al.* (31). The plasmid containing L29F/H64Q/V68F sperm whale Mb was constructed from pEMBL19 containing L29F Mb using cassette mutagenesis as described in Springer *et al.* (32). Vectors harboring the mutated gene were transformed into *Escherichia coli* strain TB1 and expressed constitutively using a 100-liter fermentor. The resulting soluble holomyoglobin protein was purified as described previously (33, 34).

Protein Crystallization—Crystals of the recombinant L29F/H64Q/V68F-Mb were grown by the batch method (35, 36) in a temperature-controlled environment (17 °C). Large single crystals developed out of solutions ranging from 2.4 to 2.7 M ammonium sulfate buffered at pH 9 (20 mM Tris-HCl, 1 mM EDTA).

X-ray Data Collection and Structure Determination—Crystals were hexagonal, space group P6, with one molecule per asymmetric unit as originally solved by Phillips *et al.* (35). They were mounted in sealed quartz capillary tubes prior to data collection. A single data set was collected from one crystal at room temperature using a Rigaku R-axis IIc imaging plate system and copper K α radiation from a Siemens rotating anode operated at 50 mV and 90 mA. The unit cell dimensions of the L29F/H64Q/V68F-metMbH₂O were $a = 91.39$, $c = 45.75$. A total of 74,100 measured reflections from 60 images ($\Delta\omega = 1.5^\circ$) with an R_{merge} of 5.7% for all data were reduced to 15,526 unique intensities (5.0 to 1.85 Å, 87.3% complete) using the program XDS.

Crystal Structure Refinement—Starting coordinates were generated using the L29F/H64Q-MbCO (Protein Data Bank entry 1MCY, Brookhaven National Laboratory) (17) to calculate initial phases. The coordinates for the additional mutated residue (V68F) were built from an electron density omit map. Solvent atoms were introduced in positive density peaks over four σ . Cycles of conventional positional refinement were carried out with XPLOR (37–39) alternated with manual fitting using the CHAIN software package (40). The crystal structures were all refined with Engh and Huber (41) topology and parameters with no restraints on the iron atom to remove bias in metal position. The crystallographic refinements converged to an R -factor of 16.8% for the triple mutant metmyoglobin structure with root mean square bond deviations of 0.017 Å. Coordinates have been deposited in the Protein Data Bank (entry 1O8M).

¹H NMR Measurements—All the ¹H NMR spectra were collected on the GE Omega 500 MHz spectrometer. The strongly relaxed signals were optimally detected in water-eliminated Fourier transform spectra (42). Nonselective T₁s for the resolved strongly relaxed protons were

measured via inversion-recovery experiment. Steady state NOEs were recorded as described previously (43). The phase-sensitive TOCSY (44, 45), NOESY (46), and conventional magnitude COSY (MCOZY) (47) employed the method described by States *et al.* (48) to provide quadrature detection in the t_1 dimension. Solvent suppression, when required, was achieved by direct saturation in the relaxation delay period. 512 blocks were collected with 25.0 kHz spectral widths to include all resonances, and 10 kHz to improve resolution for the diamagnetic envelope. 128 to 256 scans were accumulated with repetition rate of 0.7 s⁻¹ or 1.2 s⁻¹ for each block with free induction decays of 2048 complex points. The data were processed as described previously (49); details are given in the figure captions. All two-dimensional data were processed on Silicon Graphics workstation using the software package Felix from Biosym/MSI (San Diego).

Magnetic Axes Determination—The magnetic axes were determined as described previously (15, 16, 29, 30, 50). Experimental dipolar shifts for the structurally conserved proximal side of the heme were used as input to search for the Euler rotation angles, $\Gamma(\alpha, \beta, \gamma)$, that transforms the molecular pseudo-symmetry coordinates (x', y', z' , or R, θ', Ω' (Fig. 1)) readily obtained from crystal coordinates (17, 24, 25, 51) into magnetic axes, $x, y,$ and z , by minimizing the global error function,

$$\frac{F}{n} = \sum_{i=1}^n |\delta_{\text{dip}}(\text{obs}) - \delta_{\text{dip}}(\text{calc})\Gamma(\alpha, \beta, \gamma)|^2 \quad (\text{Eq. 1})$$

where

$$\delta_{\text{dip}}(\text{calc}) = \frac{1}{3N} \left[\Delta\chi_{\text{ax}}(3\cos^2\theta' - 1)R^{-3} + \frac{3}{2}(\Delta\chi_{\text{rh}} \sin^2\theta' \cos 2\Omega')R^{-3} \right] \quad (\text{Eq. 2})$$

and

$$\delta_{\text{dip}}(\text{obs}) = \delta_{\text{DSS}}(\text{obs}) - \delta_{\text{dia}} \quad (\text{Eq. 3})$$

$\Delta\chi_{\text{ax}}$ and $\Delta\chi_{\text{rh}}$ are axial and rhombic anisotropies, and $\delta_{\text{DSS}}(\text{obs})$ is the observed chemical shift referenced to DSS. δ_{dia} is the shift in the isostructural diamagnetic MbCO complex (52, 53), or calculated for protons whose δ_{dia} are not available as described in detail by Qin *et al.* (15, 16). Minimizing the error function F/n in Equation 1 was performed over three parameters, $\alpha, \beta,$ and γ , using available $\Delta\chi_{\text{ax}}$ and $\Delta\chi_{\text{rh}}$, or extended to all five parameters to yield both the Euler angles and anisotropies as described in detail previously (29).

Dipolar Shift Simulations—The position of a substituted or perturbed residue can be determined by minimizing a local error function. This local error function, designated $F^*(\text{residue})/n'$ to distinguish it from that global error function in Equation 1, is given by Ref. 30,

$$F^*(\text{residue})/n' = \sum_{i=1}^n |\delta_{\text{dip}}(\text{obs}) - \delta_{\text{dip}}(\phi, \Omega, r)|^2 \quad (\text{Eq. 4})$$

where $\delta_{\text{dip}}(\phi, \Omega, r)$ represents the $\delta_{\text{dip}}(\text{calc})$ as a function of a bond rotation ϕ or a translation of a residue by a distance r in a direction defined by the angle Ω , using the magnetic axes derived from conserved structural elements; n' is the number of residue dipolar shifts. The bond angle, ϕ , or movement defined by Ω angle and distance r , that minimize the residual error function $F^*(\text{residue})/n'$, defines structural changes as described in detail previously (15–17, 29). When available, the influence of paramagnetic relaxation, $T_1^{-1} \propto R_{\text{Fe}}^{-6}$, allowed estimate of R_{Fe} using the relation,

$$T_{1i}/T_{1j} = R_{\text{Fe}e-i}^6/R_{\text{Fe}e-j}^6 \quad (\text{Eq. 5})$$

where the His(F8) ring NH ($R_{\text{Fe}} = 5.0$ Å) and heme methyl ($R_{\text{Fe}} = 6.1$ Å) provide upper and lower limits to a proton of interest (54). The molecular modeling was carried out on a Silicon Graphics INDIGO from available crystal coordinates (17, 24, 25, 51) using the INSIGHT II (Biosym/MSI, San Diego) and MIDAS (UCSF) programs.

RESULTS

Hydrogen Sulfide and O₂ Binding to *Lucina* HbI and Sperm Whale Mb

A brief summary of the affinities of the myoglobin mutants and *Lucina* HbI for O₂ and hydrogen sulfide² is shown in Table I (17, 23, 28). *Lucina* HbI shows a 5,000-fold higher affinity for

² E. A. Brucker, G. N. Phillips, R. Lile, J. S. Olson, R. F. Eich, and J. B. Wittenberg, unpublished results.

FIG. 1. Schematic structure of the heme cavity in sperm whale mutant L29F/H64Q/V68F-Mb and *Lucina* HbI with the proximal (squares) and distal (circles) residues in contact with heme, axial His, and ligand identified by the position on helices. In cases where the residues differ for the two proteins, the residue is labeled first for L29F/H64Q/V68F-Mb and second for *Lucina* HbI. The solid lines reflect dipolar (NOESY) contacts observed for both proteins; dotted and dashed lines represent such dipolar contacts observed only in the triple mutant and *Lucina* HbI, respectively. For all but Gln⁶⁴(E7) in *Lucina* HbI, the observed dipolar contacts are completely consistent with the crystal structure of their respective aquo-met forms. The x', y', z' coordinate system represents an iron-centered coordinate system derived from crystal coordinates of MbCO. The magnetic axes, x, y, z , in which the paramagnetic susceptibility tensor is diagonal, are related by the Euler rotation $\Gamma(\alpha, \beta, \gamma)$ via $(x, y, z) = (x', y', z')\Gamma(\alpha, \beta, \gamma)$, where β represents the tilt of major magnetic axes from the heme normal, α is the direction of this tilt, defined as the angle between the projection of $-z$ on the x', y' plane and x' axis, and $\kappa \sim \alpha + \gamma$ locates the projection of the rhombic axes onto the heme plane.

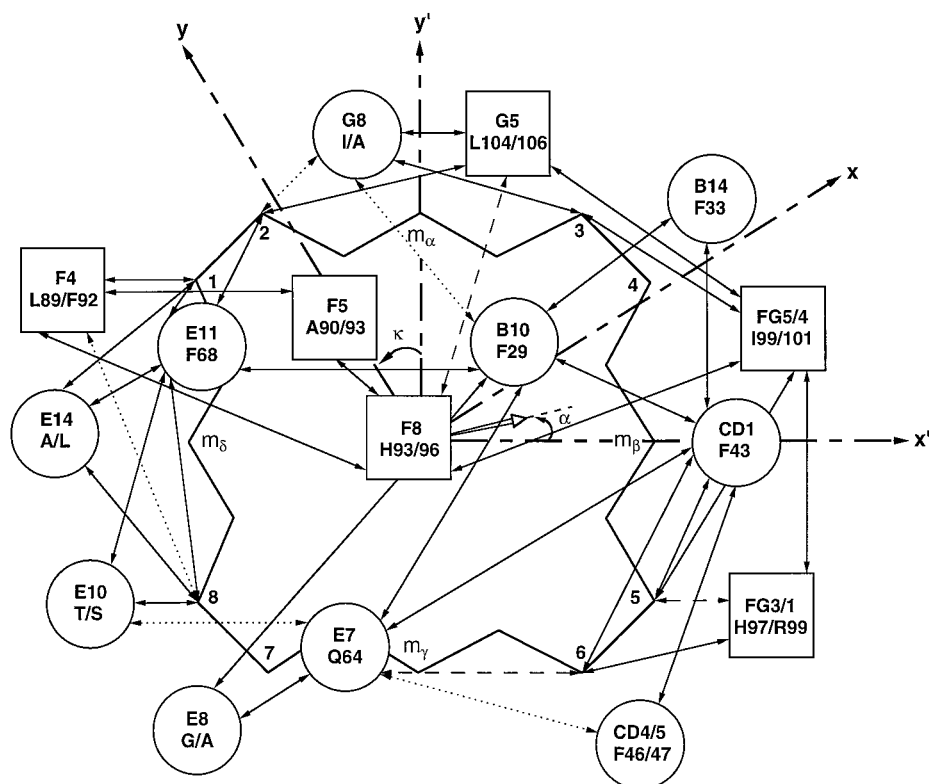


TABLE I

Equilibrium dissociation constants for O₂ and H₂S binding to *Lucina* HbI and mutants of recombinant sperm whale myoglobin

Protein	O ₂ binding to Fe(II) ^a K _{O₂}	H ₂ S binding to Fe(III) ^b K _{H₂S}	K _{H₂S} /K _{O₂}
	μM^{-1}		
<i>Lucina</i> HbI (Phe ²⁹ (B10), Gln ⁶⁴ (E7), Phe ⁶⁸ (E11))	2.5	290	116
Wild-type sperm whale Mb (Leu ²⁹ (B10), His ⁶⁴ (E7), Val ⁶⁸ (E11))	1.1	0.05	0.045
L29F-Mb	15	0.32	0.021
H64Q-Mb	0.18	1.2	6.67
V68F-Mb	0.48	0.33	0.69
L29F/H64Q-Mb	0.46	3.7	8.04
L29F/V68F-Mb	74	5.3	0.072
L29F/H64Q/V68F-Mb	3.8	37	9.74

^a References for O₂ equilibrium constants at pH 7.0, 20 °C: *Lucina* HbI (23); wild-type, L29F, H64Q, and V68F Mb (28); L29F/H64Q Mb (17); L29F/V68F and L29F/H64Q/V68F Mb.²

^b References for H₂S equilibrium constants at pH 7.5, 20 °C: *Lucina* HbI (23); wild-type and mutant myoglobins.²

sulfide than recombinant wild-type sperm whale myoglobin, whereas the two proteins have similar affinities for oxygen. There are progressive increases in K_{H₂S} as the active site of the whale myoglobin is altered to resemble that of the mollusc hemoglobin. All three single mutations, L29F, H64Q, and V68F produce large, 6–20-fold increases in sulfide affinity, and the effects on K_{H₂S} are roughly additive in the double and triple mutants. In contrast, these mutations produce markedly different effects on O₂ affinity. For example, the single H64Q and L29F mutations produces a 5-fold decrease and 15-fold increase, respectively, in O₂ affinity. As a result, K_{O₂} for the triple mutant is only 3–4-fold higher than wild-type myoglobin and very similar to that of *Lucina* HbI (Table I).

High Resolution Crystal Structure of Sperm Whale L29F/H64Q/V68F-metMbH₂O

The three mutated side chains in the recombinant myoglobin do not alter the overall tertiary structure of myoglobin nor do

they appear to sterically hinder the bound ligand. Two of these mutated residues, Gln⁶⁴(E7) and Phe⁶⁸(E11), occupy positions equivalent to those observed in the structures of corresponding H64Q-Mb and V68F-Mb single mutants (36, 55). In contrast, the aromatic ring at position 29 in the triple mutant is perpendicular to the orientation found in sperm whale L29F- and L29F/H64Q-MbCO (Fig. 2) (17, 56). A detailed comparison of the distal pockets of the L29F/H64Q/V68F-metMbH₂O and *Lucina* metHbH₂O (24) is presented in Table II and Fig. 2. The overall positions of the three mutated residues in the recombinant sperm whale metmyoglobin are close to those of the corresponding residues in the clam protein, but the exact orientations of the phenyl side chains are significantly different. The distal glutamines in both proteins form hydrogen bonds with the coordinated water molecule.

Heme Pocket Structure of L29F/H64Q/V68F-metMbCN and *Lucina* metHbICN

Resonance Assignments—The 500 MHz ¹H NMR spectra for L29F/H64Q/V28F-metMbCN, V68F-metMbCN, and *Lucina*-metHbICN in ¹H₂O at 25 °C are shown in Fig. 3, A–C, respectively. The signals for the heme for each protein were located and assigned by the characteristic pattern of dipolar contacts about the heme periphery among the TOCSY identified vinyl, propionate groups, and the pyrrole methyl, meso-Hs in a fashion standard for both diamagnetic and paramagnetic heme proteins. The pattern of heme chemical shifts is similar to that observed in wild-type sperm whale metMbCN (not shown). Resonances for residues near the heme are assigned to the degree possible, as limited by spectral congestion and paramagnetic relaxation, and by standard backbone dipolar connectivities together with characteristic TOCSY and/or COSY connectivities for several side chains (15, 16, 49). Other residues not addressable by these approaches are assigned on the basis of dipolar contacts to the heme and/or to other assigned residues. Inasmuch as this assignment strategy has been reported in detail for both wild-type and mutant metMbCN (17, 29, 30, 43),

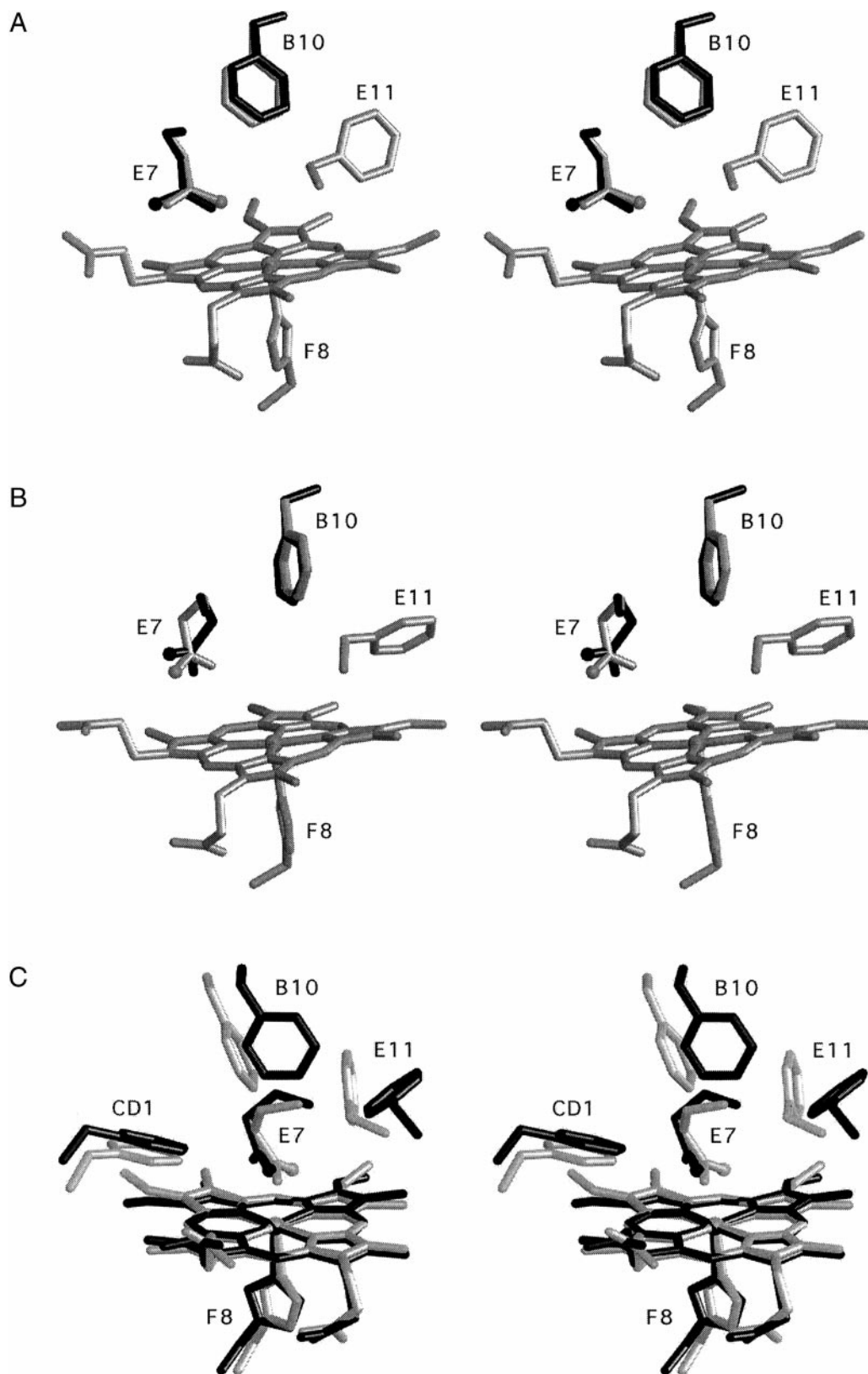


FIG. 2. Stereo diagrams of the orientations of the distal Phe(B10), Gln(E7), and Phe(E11) residues. A, L29F/H64Q/V68F-metMbCN in solution (dark lines), and L29F/H64Q/V68F-metMbH₂O in a crystal (light lines); B, *Lucina* methHbICN in solution (dark lines) and *Lucina* metHbIH₂O (24) in a crystal (light lines); C, L29F/H64Q/V68F-metMbH₂O in a crystal (light lines) and *Lucina* metHbIH₂O (24) in a crystal (dark lines); the conserved Phe⁴³(CD1) is also included in this comparison. The side chain oxygen atom of the distal glutamine is shown as a ball in each case.

two-dimensional data are shown only as relevant to the placement of perturbed distal pocket residues in both protein complexes.

The fingerprint portion of the NOESY and COSY maps (not shown) for each protein locates two extended helical fragments each, the shorter one corresponding to F helix residues F4-F9

TABLE II

Conformational parameters in the distal pockets for the aquo-met (crystal) and cyanomet (solution) structures of sperm whale L29F/H64Q/V68F-Mb and *Lucina pectinata* HbI

Distance or angle	L29F/H64Q/V68F		<i>Lucina pectinata</i>	
	MetMbCN	MetMbH ₂ O	MetHbICN	MetHbIH ₂ O ^a
Fe-Cζ(Phē ²⁹ (B10))	6.17 Å	5.97 Å	6.15 Å	6.36 Å
Fe-Nε(Gln ⁶⁴ (E7))	4.64 Å	5.98 Å	4.52 Å	4.32 Å
Fe-Cζ(Phē ⁶⁸ (E11))		6.09 Å		8.06 Å
Fe-Cζ(Phē ⁴³ (CD1))	5.30 Å	5.30 Å	5.30 Å	4.92 Å
Fe-Nε(His ⁹³ (F8))		2.19 Å		2.31 Å
Fe-OH		2.08 Å		2.28 Å
Cγ(Gln ⁶⁴ (E7))-Cζ(Phē ²⁹ (B10))	4.00 Å	3.55 Å	3.62 Å	4.87 Å
χ ₁ (Phē ²⁹ (B10))	-80°	-89°	-85°	-80°
χ ₂ (Phē ²⁹ (B10))	171°	179°	87°	87°
χ ₁ (Gln ⁶⁴ (E7))	-175°	-180°	-151°	-92°
χ ₂ (Gln ⁶⁴ (E7))	50°	49°	67°	-48°
χ ₃ (Gln ⁶⁴ (E7))	-130°	45°	168°	-98°
χ ₁ (Phē ⁶⁸ (E11))		150°		-172°
χ ₂ (Phē ⁶⁸ (E11))		66°		91°

^a Data taken from Rizzi *et al.* (24).

that includes the strongly hyperfine shifted axial His(F8). The strongly relaxed and hyperfine shifted proximal FG corner residues (His⁹⁷(FG3) and Ile⁹⁹(FG5) in Mb mutants, Arg⁹⁹(FG1) and Ile¹⁰¹(FG4) in *Lucina* HbI) are identified by their characteristic NOESY cross-peaks to the 5-CH₃. For each protein, the pattern of heme residue and inter residue dipolar contacts and paramagnetic relaxation reveal a proximal side heme pocket structure that is indistinguishable from that in the respective reference crystal structures (Fig. 1). The chemical shifts for relevant assigned resonances for the three protein complexes are listed in Table III.

The longer helical fragment represents the E helix residues E-7–E-14 in each protein, with residues E-10, E-11 and E-14 exhibiting the expected NOESY cross-peaks in the heme, including that of the Phē⁶⁸(E11) ring to the 2-vinyl group. The TOCSY/MCOSY detected fragment NHC_αH-C_βH for Gln⁶⁴(E7) in each protein shows strong NOESY cross-peaks to a moderately relaxed and hyperfine shifted CH-CH₂ fragment which is assigned to the remainder of Gln⁶⁴(E7); the C_βH-C_βH TOCSY/COSY connectivities are not observed because the cross-peak is too close to the diagonal in each protein (Figs. 4 and 5). A strongly relaxed ($T_1 \sim 12$ ms) and strongly low-field hyperfine shifted labile proton, when saturated, exhibits an intense NOE to another upfield shifted and moderately relaxed ($T_1 \sim 50$ ms) labile proton in *Lucina* metHbICN (Fig. 3E), but not detected because of overlap with the solvent signals in the triple mutant, as well as to the Gln⁶⁴(E7) C_γHs (and for the triple mutant, to Thr⁶⁷(E10); Fig. 3D) and confirms the two labile protons as arising from the N_εHs of Gln⁶⁴(E7). The T_1 s via Equation 5 reveal, $R_{Fe}(N_{\epsilon}H) = 4.2 \pm 0.2$ Å for the low-field NH for both proteins, and for *Lucina* metHbICN, the upfield resolved $R_{Fe}(N_{\epsilon}H') = 4.7 \pm 0.2$ Å. The resulting R_{Fe} are listed in Table II.

One strongly relaxed (for C_ζH) and hyperfine shifted aromatic ring with NOESY contact to 5-CH₃ and Gln⁶⁴(E7) (not shown) which uniquely identifies Phē⁴³(CD1). Another strongly hyperfine shifted and relaxed (C_ζH 19 ppm, $T_1 \sim 33$ ms) aromatic ring exhibits NOESY cross-peaks to Phē⁶⁸(E11), Gln⁶⁴(E7), Gly/Ala⁶⁵(E8), and Phē⁴³(CD1) and definitively assigns Phē²⁹(B10) for each protein (Figs. 4 and 5). The chemical shifts of relevant assigned distal residues for the three proteins are included in Table III. The pattern of dipolar contacts between distal residues and the heme, and among distal residues, are predicted by the crystal structure, as shown schematically in Fig. 1. The difference that are noted, as described below, involve primarily the residues Gln⁶⁴(E7).

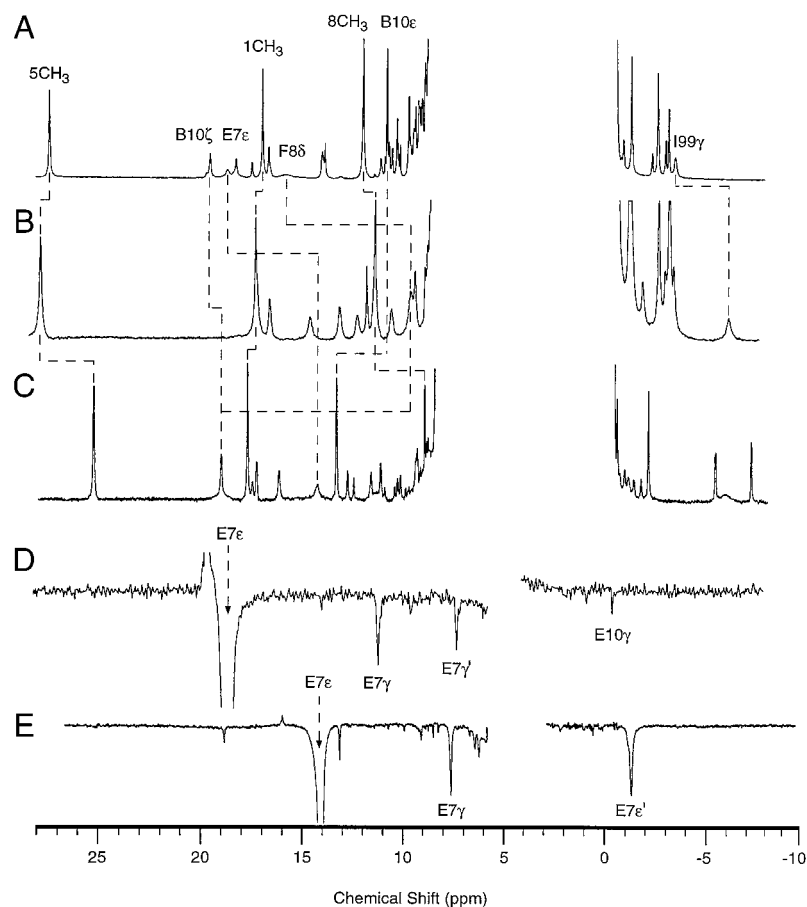
Magnetic Axes Determination—All dipolar shifted residues except Phē⁶⁸(E11) exhibit a good correlation between $\delta_{dip}(obs)$ and the slope of the chemical shift in a Curie (chemical shift versus T^{-1}) plot that is indicative of well defined orientations to the heme (not shown) (49). A variety of proximal proton dipolar shifts which correlate with their Curie slopes for each protein were used.³ To determine the magnetic axes, both as three-parameter searches for $\Gamma(\alpha, \beta, \gamma)$ using the wild-type metMbCN anisotropies, $\Delta\chi_{ax} = 2.04 \times 10^{-9}$ m³/mol, $\Delta\chi_{rh} = -0.48 \times 10^{-9}$ m³/mol (29), and as five-parameter searches for both $\Gamma(\alpha, \beta, \gamma)$ and the anisotropies. Both mutants exhibit excellent correlation between $\delta_{dip}(obs)$ and $\delta_{dip}(calc)$ with very low residual F/n in Equation 1 (not shown) typical of previous NMR studies of mutant metMbCNs (15, 16, 29, 30, 50). The chemical shifts for numerous distal residues are also well predicted. The resulting Euler angles using different input data sets were highly clustered for each protein, although distinct for each of the proteins. For L29F/H64Q/V68F-metMbCN, the optimized angles (and ranges for the various fits) are: a tilt of the major axes from the heme normal, $\beta \sim 6.3^\circ$ (6.1–6.6°), direction of tilt, $\alpha \sim -40^\circ$ (-40° to -50°) and rhombic axes, $\kappa \sim \alpha + \gamma = 30^\circ$ (20° to 40°) using MbCO crystal coordinates. The magnetic axes for V68F-metMbCN are $\alpha = 5^\circ$ (0–10°), $\beta = 7.5^\circ$ (7–8°), and $\kappa = 40^\circ$ (30–50°). The optimized anisotropies for each five-parameter fit differ inconsequentially for those of wild-type metMbCN and yield Euler angles within the ranges obtained by the 3-parameter fit (not shown). When the coordinates for L29F/H64Q/V68F-metMbCN are taken from the L29F/H64Q/V68F-metMbH₂O crystal structure presented herein, we obtain values for the angles and anisotropies that are well within the ranges obtained using the wild-type coordinates. The magnetic axes (and ranges in their values), obtained similarly for *Lucina* metMbICN, using either the *Lucina* metHbIH₂O (24) or metHbIH₂S (25) crystal coordinates, are $\beta = 7^\circ$ (6–8°), $\alpha = 155^\circ$ (150–160), $\kappa \sim \alpha + \gamma = 255^\circ$ (250–260°), and optimized anisotropies are unchanged from those of wild-type metMbCN (not shown).

Orientation of Distal Residues in L29F/H64Q/V68F-metMbCN—Using either the wild-type MbCO crystal coordinates with the mutated Phē²⁹(B10) inserted with an orientation as found in the crystal structure of L29F/H64Q-MbCO (*half-open squares* in Fig. 6A), or directly the crystal coordinates of the presently characterized L29F/H64Q/V68F-metHbH₂O (*open squares* in Fig. 6A), a qualitative, but not quantitative, correlation between $\delta_{dip}(calc)$ and $\delta_{dip}(obs)$ are observed, and the R_{Fe} (C_ζH = 4.7 Å) is shorter than indicated by $T_1 = 33$ ms ($R_{Fe} = 5.1 \pm 0.3$ Å). However, altering χ_1 by 5° from that in the L29F/H64Q-metMbCO and a 50° rotation of χ_2 leads to a Phē²⁹(B10) orientation whose $\delta_{dip}(calc)$ correlate very well with $\delta_{dip}(obs)$ (*closed squares* in Fig. 6A) and for which the R_{Fe} (C_ζH) = 5.1 Å is consistent with the T_1 value.

Introduction of Gln⁶⁴(E7) into the wild-type MbCO crystal structure based on its orientation in the H64Q-MbCO (or L29F/H64Q-MbCO) crystal structure results in reasonable agreement with both T_1 data and $\delta_{dip}(calc)$ (*half-closed circles* in Fig. 6A). However, when directly using the crystal coordinates for L29F/H64Q/V68F-metMbH₂O, neither the $\delta_{dip}(calc)$ (*open circles* in Fig. 6A) nor T_1 value for N_εH ($R_{Fe} = 5.9$ Å) are reasonably predicted ($T_1 = 14$ ms, $R_{Fe} = 4.2 \pm 0.2$). Small rotation of χ_1 (~5°) and χ_2 (~8°), followed by a 180° rotation of χ_3 for

³ The $\delta_{dip}(obs)$ used for the magnetic axes for L29F/H64Q/V68F-metMbCN and V68F-metMbCN are: Leu⁸⁹(F4) C_αH; Ala⁹⁰(F5) C_αH, C_βH₃; Phē¹³⁸(H15) C_βHs, C_εHs, C_ζH; Ile⁹⁹(FG5) C_αH, C_βH, C_γH, C_γH', C_γH₃, C_γH₃; His⁹⁷(FG3) C_αH, C_βH; and those used for *Lucina* metHbICN are: Ala⁶²(E5)-Val⁷²(E15), Phē⁹²(F4)-Ala⁹⁸(F10), Arg¹⁰¹(FG1), Gly¹⁰²(FG2), Ile¹⁰⁴(FG4), Ala¹⁰⁸(G7)-Phē¹¹⁰(G9), Val¹³⁰(H11), and Ala¹³¹(H12).

FIG. 3. 500 MHz ^1H NMR spectra of (A) L29F/H64Q/V68F-metMbCN, (B) V68F-metMbCN, and (C) *Lucina* metHbICN in $^1\text{H}_2\text{O}$ at 25 $^\circ\text{C}$, pH 7.6. Heme resonances are labeled by the Fischer notation and protein signals by the standard one-letter amino acid code. Steady-state NOE difference spectra upon saturating the low-field Gln⁶⁴(E7) N_eH peaks in: D, L29F/H64Q/V68F-metMbCN, and E, *Lucina* metHbICN.



Gln⁶⁴(E7) in the L29F/H64Q/V68F-metMbH₂O crystal structure leads to an excellent fit for $\delta_{\text{dip}}(\text{obs})$ versus $\delta_{\text{dip}}(\text{calc})$ (closed circles in Fig. 6A) and yields $R_{\text{Fe}}(\text{N}_e\text{H}) = 4.2 \text{ \AA}$, in good agreement with the 4.2- \AA value obtained from the $T_1 = 14 \text{ ms}$ via Equation 5. The other N_eH is correctly predicted to resonate close to the solvent signal by the optimized $\delta_{\text{dip}}(\text{calc})$. Similarly small variations in χ_1 , χ_2 starting with the Gln⁶⁴(E7) orientation in the single mutant lead to a Gln orientation essentially the same as that obtained starting with the coordinate of the triple mutant (not shown).

The anomalous variable temperature slopes (see above), small $\delta_{\text{dip}}(\text{calc})$ which are relatively insensitive to ring orientation, and the presence of comparable magnitude but opposed sign $\delta_{\text{dip}}(\text{calc})$ and ring current shift rendered the optimization of the orientation of Phe⁶⁸(E11) ring on the basis of $\delta_{\text{dip}}(\text{obs})$ completely impractical (50). The pattern of small δ_{dip} for Phe⁶⁸(E11), nevertheless, are consistent with observed dipolar shifts and NOESY contacts. The orientation for these three mutated residues in L29F/H64Q/V68F-metMbCN are shown in Fig. 2A, and the relevant side chain bond angles and distances to the iron are listed in Table II.

Orientation of Distal Residues in *Lucina* MetHbICN—The orientations for Gln⁶⁴(E7) in the *Lucina* metMbH₂O (24) or metHbIH₂S (25) crystal structures yielded completely unacceptable fits for $\delta_{\text{dip}}(\text{obs})$ versus $\delta_{\text{dip}}(\text{calc})$ for *Lucina*-metMbICN in solution (as shown by open circles and half-closed circles, respectively, in Fig. 6B); the correlation is particularly poor for the labile N_eHs where both models predict even the wrong sign for $\delta_{\text{dip}}(\text{calc})$. Moreover, the low-field N_eH closest to the iron has $R_{\text{Fe}} \sim 3.5 \text{ \AA}$ and 5.2 \AA in the two crystal structures while the observed $T_1 = 12 \text{ ms}$ predicts $R_{\text{Fe}} \sim 4.2 \pm 0.2 \text{ \AA}$ via Equation 5. Since the Gln⁶⁴(E7) orientation in *Lucina* metHbIH₂O had the N_eH oriented toward the ligated water,

which is expected to be a H-bond donor, the Gln orientation with χ_3 rotated by 180 $^\circ$ to interchange the carbonyl and amide groups was considered. This altered orientation leads to different N_eH₂ dipolar shifts (not shown) that fit $\delta_{\text{dip}}(\text{obs})$ better, but still unacceptably. Attempts to obtain a fit for $\delta_{\text{dip}}(\text{obs})$ by sequential χ_1 , χ_2 , χ_3 rotation failed since $\delta_{\text{dip}}(\text{calc})$ for C _{β} Hs is quite insensitive to the χ_1 . Instead, the combination of the large low-field $\delta_{\text{dip}}(\text{obs})$ and $R_{\text{Fe}} \sim 4.2 \text{ \AA}$ (from the $T_1 = 12 \text{ ms}$) was used to uniquely locate the low-field N_eH in the crystal coordinates, and a search made for the position in space of the other N_eH (with intra N_eH distance 1.88 \AA) to satisfy both the upfield $\delta_{\text{dip}}(\text{obs})$ and $R_{\text{Fe}} \sim 4.6 \pm 0.2 \text{ \AA}$ obtained from its $T_1 = 22 \text{ ms}$. Upon obtaining a reasonable fit for the N_eHs that satisfy both relaxation and $\delta_{\text{dip}}(\text{obs})$ constraints, a search was pursued for the range of χ_1 , χ_2 , and χ_3 allowed by the fixed C _{α} H and NH₂ positions. The good correlation between $\delta_{\text{dip}}(\text{calc})$ and $\delta_{\text{dip}}(\text{obs})$ for this optimized Gln orientation is shown in Fig. 6B (closed circles). The resulting torsional angles for Gln⁶⁴(E7) are listed in Table II where they are compared with values in the crystal structure of *Lucina* metHbIH₂O.

The orientation of Phe²⁹(B10) in the crystal structures of either *Lucina* metHbIH₂O (24) or metHbIH₂S (25) yield very similar ring proton $\delta_{\text{dip}}(\text{calc})$ that correlate equally well with $\delta_{\text{dip}}(\text{obs})$ (open and closed squares in Fig. 6B, respectively). The crystallographic $R_{\text{Fe}}(\text{C}_\alpha\text{H})$ (5.6 \AA), however, is somewhat larger than the value reflected in its $T_1 \sim 40 \text{ ms}$ ($R_{\text{Fe}} = 5.2 \pm 0.2 \text{ \AA}$ via Equation 5). A $\sim 5^\circ$ change in χ_1 alters the $\delta_{\text{dip}}(\text{calc})$ inconsequentially but results in a reasonable $R_{\text{Fe}}(\text{C}_\alpha\text{H}) \sim 5.3 \text{ \AA}$. Phe⁶⁸(E11) exhibits only minor $\delta_{\text{dip}}(\text{obs})$ and, like in the triple mutant Mb, yields anomalous Curie plots that reflect variable population of alternate orientations (50). The crystallographic orientation, however, is consistent both with $\delta_{\text{dip}}(\text{calc})$ (not shown) and NOESY cross-peak pattern (Fig. 1). It is noted that

TABLE III
¹H NMR chemical shifts of the amino acid residues in sperm whale L29F/H64Q/V68F-metMbCN and V68F-metMbCN and in *Lucina metHbICN*

Chemical shifts in ppm at 25 °C (L29F/H64Q/V68F-metMbCN and *Lucina metHbICN*) and at 30 °C (V68F-metMbCN), pH 7.2, reference to DSS.

Residues	Peaks	L29F/H64Q/V68F-metMbCN	V68F-metMbCN	<i>Lucina metHbICN</i>
Phe ²⁹ (B10)	Ring ^a	8.28, 10.73, 19.49	5.38, 3.98, 4.48	8.70, 13.07, 18.77
Phe ⁴³ (CD1)	Ring ^a	7.48, 9.42, 11.95	7.55, 9.54, 11.92	6.40, 6.20, 7.26
Gln ⁶⁴ (E7)	NpH	9.16		8.93
	CαH	5.88		4.62
	CβHs	5.56, 4.33		3.03, 3.29
	CγHs	11.12, 7.19	11.65	7.63, 4.97
	NεHs	18.67, 5 ± 1		14.05, -1.39
Thr ⁶⁷ (E10)/Ser ⁶⁷ (E10)	NpH	9.34		8.58
	CαH	3.34	2.78	3.59
	CβH	5.22	3.38	2.16
	CγH ₃ /CβH'	-0.59	-1.00	3.45
Phe ⁶⁸ (E11)	NpH	10.61		9.89
	CαH	1.80	-1.02	3.81
	CβHs	6.27, 5.22	2.84	9.05, 6.40
	Ring ^a	8.85, 6.81, 7.67	8.57, 8.07, 7.88	7.47, 7.53, 7.87
Ala ⁷¹ (E14)/Leu ⁷¹ (E14)	NpH	6.11		6.03
	CαH	3.26	3.36	3.04
	CβH ₃ /CβHs	-0.66	-0.41	-0.86, -0.69
	CγH			-2.01
	CδH _{3,s}			-2.36, -0.83
Leu ⁸⁹ /Phe ⁹² (F4)	NpH	7.26		7.89
	CαH	6.63	7.56	5.98
Ala ^{90/93} (F5)	NpH	10.23		9.64
	CαH	6.42	6.26	5.60
	CβH ₃	2.53	2.51	2.31
His ^{93/96} (F8)	NpH	13.89		12.52
	CαH	9.34	9.17	10.86
	CβHs	13.93, 9.64	12.64, 7.97	11.34, 9.13
	CγH	15.83	10.10	18.79
	CεH	4.5 ± 2.5		-6.14
	NγH	18.23		15.94
His ⁹⁷ (FG3)/Arg ⁹⁹ (FG1)	Ring ^b /CδHs	13.00, 6.76	13.80, 7.20	4.26, 6.61
Ile ⁹⁹ (FG5)/Ile ¹⁰¹ (FG4)	CαH	3.35	2.98	4.07
	CβH	2.68	1.41	3.07
	CγHs	-3.53, 1.33	-5.46, 0.49	
	CγH ₃	-1.38	-2.33	0.50
	CδH ₃	-2.71	-2.83	0.83
Ile ¹⁰⁷ (G8)/Ala ¹⁰⁹ (G8)	NpH			6.84
	CγH'/CαH	0.24		3.61
	CδH ₃ /CβH ₃	-0.54		0.23
Phe ¹³⁸ (H15)	Ring ^a	6.84, 6.97, 7.11	7.08, 6.62, 7.08	

^a For Phe ring protons, the shifts are listed as: CδHs, CεHs, and CζH.

^b For His ring proton, the shifts are listed as CδH and CεH.

for *Lucina metHbICN*, in contrast to L29F/H64Q/V68F-metMbCN, the crystallographic distal Phe⁴³(CD1) placement in either crystal structure yields similarly poor fits for δ_{dip}(obs) versus δ_{dip}(calc) (open triangles in Fig. 6B). Moreover, the Gln⁶⁴(E7) orientation deduced above results in a ~0.3 Å van der Waals overlap with the crystallographically defined Phe⁴³(CD1) ring. Moving the Phe⁴³(CD1) ring 0.3 Å parallel to the heme so as to abolish this steric interaction leads to a much better fit between δ_{dip}(obs) and δ_{dip}(calc) for Phe⁴³(CD1) (closed triangles, Fig. 6B). The positions of the distal residues for metHbIH₂O in the crystal and metHbICN in solution are compared in Fig. 2B, and reveal significant differences primarily for the Gln⁶⁴(E7) orientation.

DISCUSSION

Solution NMR Cavity Structure—The conventional two-dimensional NMR approach allowed unambiguous assignment for all relevant residues in the heme cavity. The intrinsic paramagnetism of cyano-metMb, instead of being an impediment to assignment, was actually an advantage since the dipolar shift with minimal relaxation provide significantly enhanced resolution for the E and F helical segments. For the proximal side of the heme, the NOESY cross-peak patterns and paramagnetic relaxation for the two Mb mutants were indistinguishable from those observed for wild-type metMbCN and predicted by the

wild-type MbCO structure. A similarly strongly conserved proximal structure is confirmed for *Lucina metHbICN*. These conserved proximal structures allow the determination of meaningful magnetic axes for each protein. The robust nature of the magnetic axes for L29F/H64Q/V68F-metMbCN is confirmed by the indistinguishable magnetic axes determined using either the wild-type MbCO or triple mutant crystal structures.

For the distal residues, whose relaxation properties, dipolar shifts and/or NOESY cross-peak pattern differed from that expected for the reference crystal structure, the combined restraints for dipolar shifts and paramagnetic relaxation allow the determination of their orientations in a more definitive manner than allowed by the NOESY cross-peak pattern themselves. The accuracy of the distal orientations is limited only by the basic assumption that the helical backbone positions are inconsequentially perturbed in the mutant and/or ligation variant relative to the available crystal structure. It is noted that the labile protons of the distal Gln⁶⁴(E7) are readily assigned. The combined effect of the dipolar shift and paramagnetic relaxation allow the placement of the labile protons in the distal pocket so as to more accurately describe hydrogen bonding between Gln⁶⁴(E7) and the bound ligand than is possible in some of the crystal structures.

FIG. 4. Portions of the MCOSEY (A, A') and NOESY ($\tau_m = 50$ ms) (B, B') spectra of *Lucina* metHbCN in $^2\text{H}_2\text{O}$ at 25 °C, pH 7.0, showing the identification of the Phe²⁹(B10) and Gln⁶⁴(E7) spin system and the relevant dipolar contact between the two residues. The MCOSEY data were processed by applying 512 $t_1 \times 512 t_2$ points prior to zero filling to 2048 \times 2048 data points and Fourier transformation. The NOESY data were processed by applying 30°-shifted sine-bell squared window over 1024 $t_1 \times 256 t_2$ prior to zero-filling to 2048 \times 2048 data points and Fourier transformation.

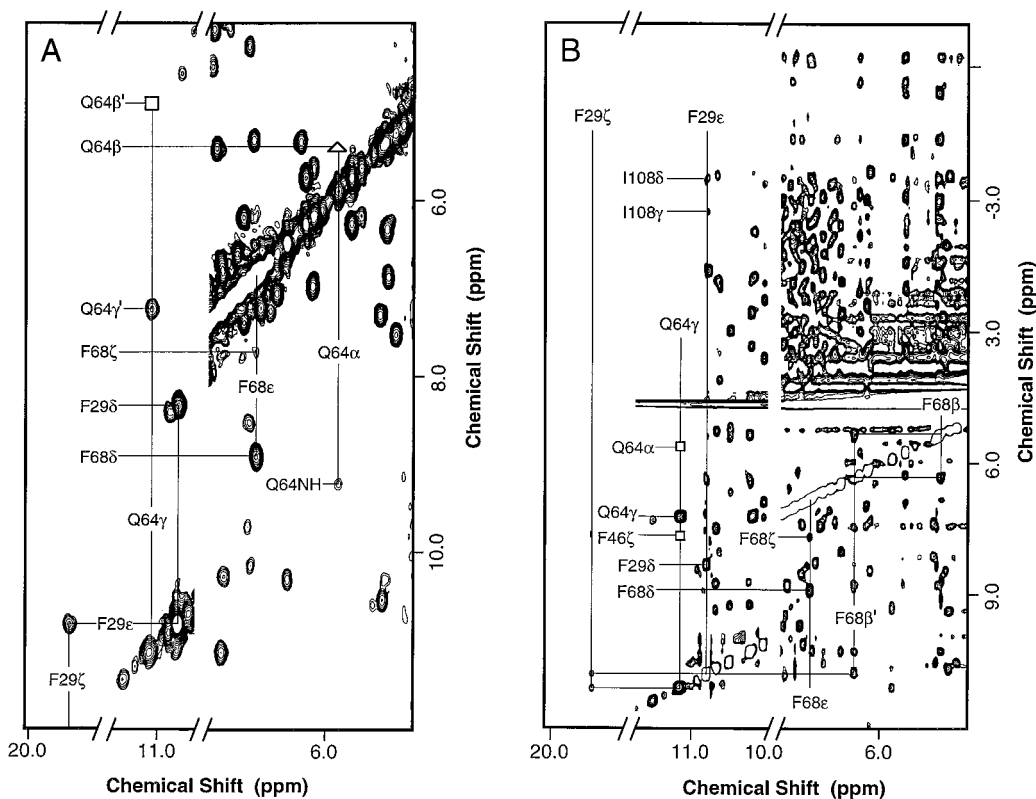
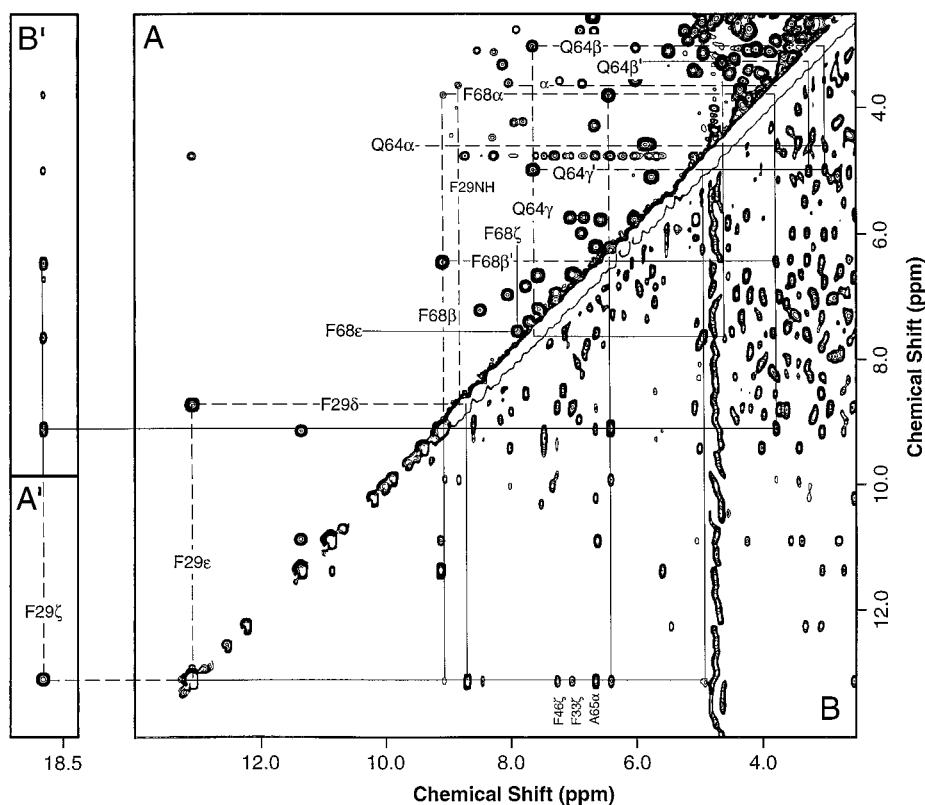


FIG. 5. Portions of the MCOSEY (A) and NOESY ($\tau_m = 50$ ms) (B) spectra of L29F/H64Q/V68F-metMbCN in $^1\text{H}_2\text{O}$ at 25 °C, pH 7.0, showing the identification of the Phe²⁹(B10) and Gln⁶⁴(E7) spin system and the relevant dipolar contact between the two residues. MCOSEY and NOESY data were processed as described in detail in the legend to Fig. 4.

The aromatic ring for Phe⁶⁸(E11) is oriented away from the expected binding site with the ring inserting into a largely pre-existing cavity in the distal pocket (55). The absence of a methyl group at the γ_2 position results in less direct hindrance of the bound ligand than is observed for the naturally occurring

Val side chain. Thus, the Phe⁶⁸(E11) mutant behaves like V68A-metMbCN; both exhibit less tilt, $\beta \sim 7\text{--}9^\circ$, than that in the wild-type protein ($\beta = 16^\circ$) (30, 57). Last, the labile Gln⁶⁴(E7) protons are in a position to form hydrogen bonds with bound cyanide in the distal pockets of both L29F/H64Q/

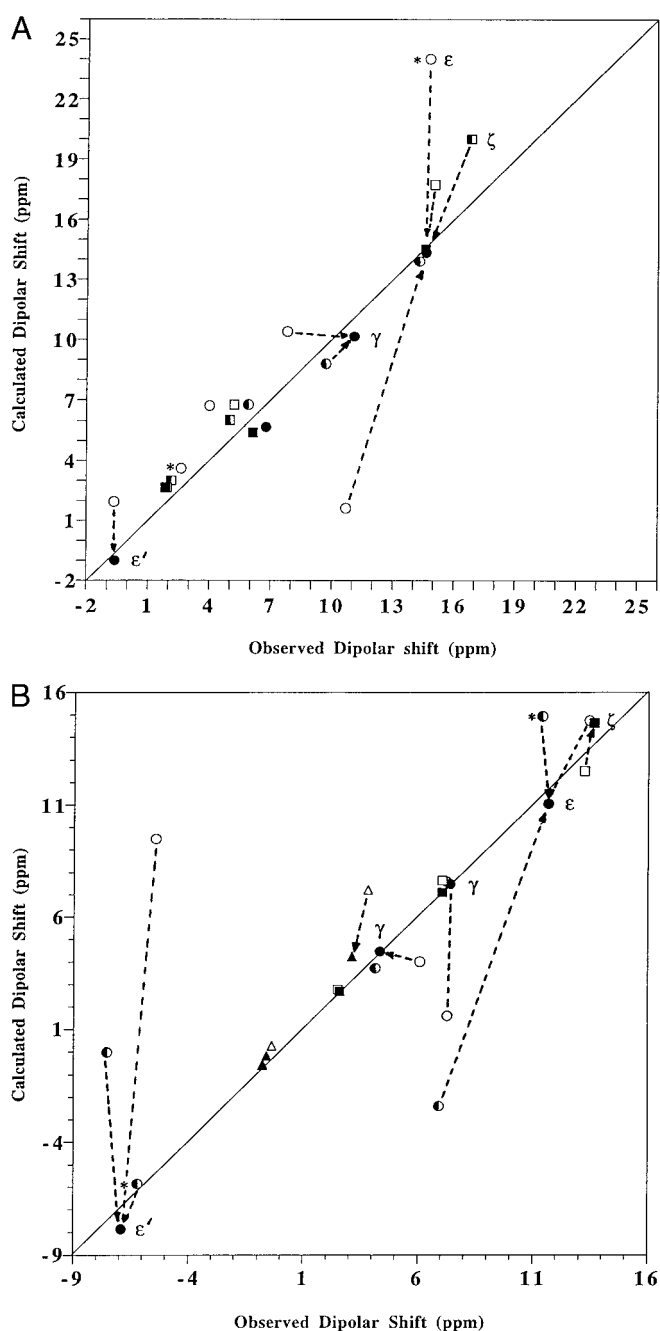


FIG. 6. Plot of $\delta_{\text{dip}}(\text{obs})$ versus $\delta_{\text{dip}}(\text{calc})$ for key distal residues. A, L29F/H64Q/V68F-metMbCN for Phe²⁹(B10) (squares) and Gln⁶⁴(E7) (circles) based on the L29F/H64Q-MbCO crystal structure (half-filled marker), L29F/H64Q/V68F-metMbH₂O (open marker) crystal structures, and the latter crystal structures with Gln⁶⁴(E7) χ_3 rotated by 180° (open marker with asterisk) as determined by NMR (closed markers); B, *Lucina* metHbICN for Phe²⁹(B10) (squares), Gln⁶⁴(E7) (circles) and Phe⁴³(CD1) (triangles) based on the crystal structures of *Lucina* metHbIH₂O (24) (open markers), the crystal structure of *Lucina* metHbIH₂S (25) (half-closed markers) and with Gln⁶⁴(E7) χ_3 rotated by 180° (half-closed markers with asterisk), and as determined by NMR (closed markers).

V68F metMbCN and *Lucina* metHbICN. This orientation is probably similar to that in the oxy complexes.

Comparison of Distal Pockets in Solution and Crystal Structures—For all but select distal residues, the heme pocket structure for each protein is essentially the same in cyanomet and aquo-met derivatives. In the case of the sperm whale triple mutant, the major difference in the Gln⁶⁴(E7) orientation between the cyanomet and aquomet complexes is $\sim 180^\circ$ rotation

about χ_3 that interchanges the carboxy and amide termini (Table II, Fig. 2A). The 180° rotation of the Gln side chain terminus is completely consistent with the stabilizing roles of the side chain for the different ligands. For the cyano complex, the N_eH₂ is oriented to serve as a H-bond donor to bound cyanide, whereas in the aquomet complex, the carbonyl oxygen is oriented to accept a H-bond from coordinated water. The small changes in χ_1 , χ_2 for Gln⁶⁴(E7) (Table II) help to accommodate the larger cyanide ligand.

As shown in Fig. 2B, the solution orientation of Gln⁶⁴(E7) in *Lucina* metHbCN I differs substantially from that reported for the corresponding aquomet crystal. The altered orientation is firmly and independently established by the NOESY pattern from C_γHs to Phe²⁹(B10), the dipolar shift simulation, and the paramagnetic relaxation. However, both structures place the amino group in a position to interact with the bound ligand. The electron density in the crystal structure does not allow differentiation between the terminal carbonyl O atom and the N_e atom.⁴ However, the carbonyl O atom rather than the reported NH₂ must be pointing toward the coordinated water to serve as H-bond acceptor. Donation of proton to the bound water would give the ligand a partial positive charge (*i.e.* H₃O⁺ character) causing substantial electrostatic repulsion with the net +1 charge on the heme iron atom. Thus, the solution NMR data, through the dipolar shift and paramagnetic relaxation, provide the most definitive location of the NH₂ group. The small movements of Phe²⁹(B10) and Phe⁴³(CD1) in *Lucina* HbI appear to reflect minor accommodation of the larger cyanide ligand. However, the orientations of Gln⁶⁴(E7) do differ in solution and crystal, as shown in Fig. 2B.

The orientation of the Gln⁶⁴(E7) side chain in the sulfide complex of *Lucina* metHbI (not shown) is intermediate between that for the aquomet crystal and that for metHbICN in solution (Fig. 2B). The CO *versus* NH₂ terminus orientation in the sulfide complex of *Lucina* metHbI also differs from that in metHbICN in solution by a 180° rotation at χ_3 . Again, this difference is consistent hydrogen bond donation to bound cyanide and acceptance from bound H₂S.

Implications for Sulfide Binding—All three single distal pocket substitutions in sperm whale Mb cause an enhancement of sulfide binding but have variable effects on oxygen affinity. The key mutation is H64Q, which causes a 25-fold increase in sulfide affinity by itself. The triple mutant, L29F/H64Q/V68F-metMb, has a sulfide affinity which is ~ 700 times greater than that of wild-type metMb and only ~ 7 -fold less than that of *Lucina* HbI. Thus the triple mutant exhibits an increased sulfide binding free energy of ~ 3.8 kcal/mol or about $\sim 75\%$ of the stabilization of the bound sulfide (~ 5.1 kcal/mol) by native *Lucina* HbI relative to that by wild-type sperm whale Mb. Hence, a major portion, but not all, of the remarkable sulfide affinity of *Lucina* HbI can be transferred to a mammalian Mb by replacing the three residues in contact with bound sulfide with those found in *Lucina* HbI. The high affinity of *Lucina* HbI for sulfide was attributed (24, 25) to a combination of the hydrogen-bond acceptance by the Gln⁶⁴(E7) side chain carbonyl, the hydrophobic pocket provided by the “cage” generated by the three Phe side chains, B10, CD1, and E11, and highly favorable electrostatic interactions between the sulfur and the edges of the three aromatic rings. While the distal pockets for the triple mutant Mb and *Lucina* HbI are similar (Fig. 2), there are some significant differences that relate to their differences in affinity for sulfide.

The side chains of Gln⁶⁴(E7) and Phe⁴³(CD1) have similar orientations in the sperm whale triple mutant and the clam

⁴ M. Bolognesi, personal communication.

protein (Fig. 2C). However, both Phe²⁹(B10) and Phe⁶⁸(E11) in the sperm whale mutant are rotated $\sim 90^\circ$ about χ_2 relative to their positions in *Lucina* HbI and their edges are closer to the iron atom in the mollusc Hb (Fig. 2C). As a result of the differences, *Lucina* hemoglobin has a significantly larger ligand-binding site than that found in the myoglobin mutants, which should facilitate the binding of the large H₂S ligand. The change in orientation of Phe²⁹(B10) should have little effect on stabilization of bound sulfide since the positive edge of the ring multipole is pointing toward the bound ligand in both proteins. In *Lucina* HbI, the positive edge of the Phe⁶⁸(E11) ring also points toward the bound ligand (Fig. 2C). This orientation of the Phe(E11) side chain is caused by direct steric interactions Phe²⁸(B9) in *Lucina* HbI (25). Stabilization of bound sulfide by Phe⁶⁸(E11) ring does not appear to occur in the myoglobin triple mutant since the E-11 side chain is allowed to take a position more perpendicular to the plane of the heme since the B9 position is occupied by a smaller Ile residue. A more complete and quantitative interpretation of the sulfide binding data will require detailed volume and electrostatic calculations for the entire set of mutants listed in Table I; such studies are now in progress.

Acknowledgments—We thank Eileen Singleton for the expression and purification of the triple mutant myoglobin, Mike Berry for help in the protein's crystallization and subsequent structural refinement, and Jun Qin for assistance with NMR experiments.

REFERENCES

- Lesk, A. M., and Chothia, C. (1980) *J. Mol. Biol.* **136**, 225–270
- Bashford, D., Chothia, C., and Lesk, A. M. (1987) *J. Mol. Biol.* **196**, 199–216
- Vinogradov, S. N., Walz, D. A., Pohajdak, B., Moens, L., Kapp, O. H., Susuzki, T., and Trotman, C. N. A. (1993) *Comp. Biochem. Physiol.* **106**, 1–26
- Romero-Herrera, A. E., Goodman, M., Dene, H., Bartiniki, D. E., and Mizukami, H. (1981) *J. Mol. Evol.* **17**, 140–147
- Suzuki, T., Muramatsu, R., Kisamori, T., and Furukohri, T. (1988) *Zool. Sci.* **5**, 69–76
- Liljeqvist, G., Paléus, S., and Braunitzer, G. (1982) *J. Mol. Evol.* **18**, 102–108
- Stenzel, P., Brimhall, B., Jones, R. T., Black, J. A., McLachlan, A., and Gibson, D. (1979) *J. Biol. Chem.* **254**, 2071–2076
- Bolognesi, M., Onesti, S., Gatti, G., Coda, A., Ascenzi, P., Giacometti, A., and Brunori, M. (1989) *J. Mol. Biol.* **205**, 529–544
- Suzuki, T., Furukohri, T., and Okamoto, S. (1993) *J. Protein Chem.* **12**, 45–50
- Rashid, K. A., Van Hauwaert, M.-L., Haque, M., Siddiqi, A. H., Lasters, I., De Mayer, M., Griffon, N., Marden, M. C., Dewilde, S., Clauwaert, J., Vinogradov, N., and Moens, L. (1997) *J. Biol. Chem.* **272**, 2992–2999
- Zhang, W., Rashid, K. A., Haque, M., Siddiqi, A. H., Vinogradov, S. N., Moens, L., and La Mar, G. N. (1997) *J. Biol. Chem.* **272**, 3000–3006
- Arents, G., and Love, W. E. (1989) *J. Mol. Biol.* **210**, 149–161
- Travaglini Allocatelli, C., Cutruzzolá, F., Brancaccio, A., Brunori, M., Qin, J., and La Mar, G. N. (1993) *Biochemistry* **32**, 6041–6049
- Vyas, K., Rajarathnam, K., Yu, L. P., Emerson, S. D., La Mar, G. N., Krishnamoorthi, R., and Mizukami, H. (1993) *J. Biol. Chem.* **268**, 14826–14835
- Qin, J., La Mar, G. N., Ascoli, F., and Brunori, M. (1993) *J. Mol. Biol.* **231**, 2009–2023
- Qin, J., La Mar, G. N., Cutruzzolá, F., Travaglini Allocatelli, C., Brancaccio, A., and Brunori, M. (1993) *Biophys. J.* **65**, 2178–2190
- Zhao, X., Vyas, K., Nguyen, B. D., Rajarathnam, K., La Mar, G. N., Li, T., Phillips, G. N., Jr., Eich, R. F., Olson, J. S., Ling, J., and Bocian, D. F., (1995) *J. Biol. Chem.* **270**, 20763–20774
- Wittenberg, J. (1985) *Bull. Biol. Soc. Wash.* **6**, 301–310
- Wittenberg, J. B. and Wittenberg, B. A. (1990) *Annu. Rev. Biochem. Biophys. Commun.* **19**, 217–241
- Wittenberg, J. B. and Kraus, D. W. (1991) in *Structure and Function of Invertebrate Oxygen Carriers* (Vinogradov, S. N., and Kapp, O. H., eds) pp. 323–330, Springer Verlag, New York
- Fisher, C. R. (1990) *Revs. Aquat. Sci.* **2**, 399–446
- Childress, J. J., and Fisher, C. R. (1992) *Oceanogr. Marine Biol. Annu. Rev.* **30**, 337–441
- Kraus, D. W., and Wittenberg, J. B. (1990) *J. Biol. Chem.* **265**, 16043–16053
- Rizzi, M., Wittenberg, J. B., Coda, A., Fasano, M., Ascenzi, P., and Bolognesi, M. (1994) *J. Mol. Biol.* **244**, 86–89
- Rizzi, M., Wittenberg, J. B., Coda, A., Ascenzi, P., and Bolognesi, M. (1996) *J. Mol. Biol.* **258**, 1–5
- Zhang, W., Cutruzzolá, F., Travaglini Allocatelli, C., Brunori, M., and La Mar, G. N. (1997) *Biophys. J.* **73**, 1019–1030
- Bisig, D. A., Di Iorio, E. E., Diederichs, K., Winterhalter, K. H., and Pionteck, K. (1995) *J. Biol. Chem.* **270**, 20754–20762
- Springer, B. A., Sligar, S. G., Olson, J. S., and Phillips, G. N., Jr. (1994) *Chem. Rev.* **94**, 699–714
- Rajarathnam, K., La Mar, G. N., Chiu, M., and Sligar, S. G. (1992) *J. Am. Chem. Soc.* **114**, 9048–9058
- Rajarathnam, K., Qin, J., La Mar, G. N., Chiu, M. L., and Sligar, S. G. (1993) *Biochemistry* **32**, 5670–5680
- Egeberg, K. D., Springer, B. A., Sligar, S. G., Carver, T. E., Rohlf, R. J., and Olson, J. S. (1990) *J. Biol. Chem.* **265**, 11788–11795
- Springer, B. A., Egeberg, K. D., Sligar, S. G., Rohlf, R. J., Mathews, A. J., and Olson, J. S. (1989) *J. Biol. Chem.* **264**, 3057–3060
- Carver, T. E., Brantley, R. E., Jr., Singleton, E. W., Arduini, R. M., Quillin, M. L., Phillips, G. N., Jr., and Olson, J. S. (1992) *J. Biol. Chem.* **267**, 14443–14450
- Springer, B. A., and Sligar, S. G. (1987) *Proc. Natl. Acad. Sci. U. S. A.* **84**, 8961–8965
- Phillips, G. N., Jr., Arduini, R. M., Springer, B. A., and Sligar, S. G. (1990) *Proteins Struct. Funct. Genet.* **7**, 358–365
- Quillin, M. L., Arduini, R. M., Olson, J. S., and Phillips, G. N., Jr. (1993) *J. Mol. Biol.* **234**, 140–155
- Brünger, A. T., Kuriyan, J., and Karplus, M., (1987) *Science* **235**, 458–460
- Brünger, A. T., Karplus, M., and Petsko, G. A. (1989) *Acta Crystallogr. Sec. A* **45**, 50–61
- Brünger, A. T. (1992) *X-PLOR Version 3.1 Manual*, Yale University
- Sack, J. S. (1988) *J. Mol. Graph.* **6**, 244–245
- Engh, R. A., and Huber, R. (1991) *Acta Crystallogr. Sec. A* **47**, 392–400
- Gupta, R. K. (1976) *J. Magn. Res.* **24**, 461–465
- Emerson, S. D., and La Mar, G. N. (1990) *Biochemistry* **29**, 1545–1556
- Braunschweiler, L., and Ernst, R. R. (1983) *J. Magn. Reson.* **53**, 521–528
- Davis, D. G., and Bax, A. (1985) *J. Am. Chem. Soc.* **107**, 2820–2821
- Jeener, J., Meier, B. H., Bachmann, P., and Ernst, R. R. (1979) *J. Chem. Phys.* **71**, 4546–4553
- Bax, A. (1982) *Two-dimensional Nuclear Magnetic Resonance in Liquids*, Delft University Press, Dordrecht, Holland
- States, D. J., Haberkorn, R. A., and Reuben, D. J. (1982) *J. Magn. Reson.* **48**, 286–292
- Qin, J., and La Mar, G. N. (1992) *J. Biomol. NMR* **2**, 597–618
- Emerson, S. D., and La Mar, G. N. (1990) *Biochemistry* **29**, 1556–1566
- Kuriyan, J., Witz, S., Karplus, M., and Petsko, G. A. (1986) *J. Mol. Biol.* **192**, 133–154
- Dalvit, C. G., and Wright, P. E. (1987) *J. Mol. Biol.* **194**, 313–327
- Chiu, M. L. (1992) *Structure and Dynamics of Myoglobin and its Mutants*, Ph.D. thesis, University of Illinois, Urbana, IL
- Zhang, W., La Mar, G. N., and Gersonde, K., (1996) *Eur. J. Biochem.* **237**, 841–853
- Quillin, M. L., Li, T., Olson, J. S., Phillips, G. N., Jr., Dou, Y., Ikeda-Saito, M., Regan, R., and Gibson, Q. H. (1995) *J. Mol. Biol.* **245**, 416–436
- Carver, T. E., Rohlf, R. J., Olson, J. S., Gibson, Q. H., Blackmore, R. S., Springer, B. A., and Sligar, S. G. (1990) *J. Biol. Chem.* **265**, 20007–20020
- Rajarathnam, K., Qin, J., La Mar, G. N., Chiu, M. L., and Sligar, S. G. (1994) *Biochemistry* **33**, 5493–5501